JACS
JOURNAL OF THE AMERICAN CHEMICAL SOCIETY
Article
pubs.acs.org/JACS

A Mechanistic Investigation of the Gold(III)-Catalyzed Hydrofurylation of C−C Multiple Bonds

Amin Hossein Bagi,[†] Yousef Khaledi,[†] Hossein Ghari,[†] Sebastian Arndt,[‡] A. Stephen K. Hashmi,*[,‡] Brian F. Yates,*[,§] and Alireza Ariafard*[,†,§]

[†]Department of Chemistry, Faculty of Science, Central Tehran Branch, Islamic Azad University, Shahrak Gharb, Tehran 1467686831, Iran

[‡]Organisch-Chemisches Institut, Universität Heidelberg, Im Neuenheimer Feld 270, Heidelberg 69120, Germany

[§]School of Physical Sciences (Chemistry), University of Tasmania, Private Bag 75, Hobart, Tasmania 7001, Australia

Supporting Information

ABSTRACT: The gold-catalyzed direct functionalization of aromatic C−H bonds has attracted interest for constructing organic compounds which have application in pharmaceuticals, agrochemicals, and other important fields. In the literature, two major mechanisms have been proposed for these catalytic reactions: inner-sphere *syn*-addition and outer-sphere *anti*-addition (Friedel−Crafts-type mechanism). In this article, the $AuCl_3$-catalyzed hydrofurylation of allenyl ketone, vinyl ketone, ketone, and alcohol substrates is investigated with the aid of density functional theory calculations, and it is found that the corresponding functionalizations are best rationalized in terms of a novel mechanism called "concerted electrophilic ipso-substitution" (CEIS) in which the gold(III)-furyl σ-bond produced by furan auration acts as a nucleophile and attacks the protonated substrate via an outer-sphere mechanism. This unprecedented mechanism needs to be considered as an alternative plausible pathway for gold(III)-catalyzed arene functionalization reactions in future studies.

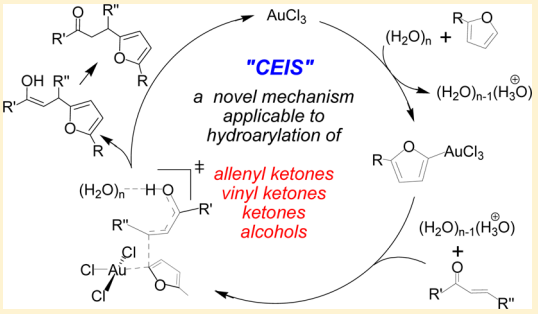

INTRODUCTION

Gold-catalyzed reactions for the synthesis of valuable chemicals have recently experienced significant interest. The C−H bond functionalization of aromatic compounds is one of the most important transformations catalyzed by gold complexes.[1] This catalytic process was developed for the first time by Hashmi and co-workers in 2000.[2] They demonstrated that terminal allenyl ketone **I** in the presence of $AuCl_3$ catalyst is easily converted to a mixture of the furan **II** and the vinyl ketone **III** (eq 1). The authors subsequently observed that $AuCl_3$ slowly catalyzes the reaction of furan **II** with vinyl ketone **III** to produce ketone **IV**. Interestingly, Hashmi et al. reported that the addition of vinyl ketone **V** to a solution of $AuCl_3$ and allenyl ketone **I** only affords **VI**, and neither **II** nor **III** is formed during the course of this reaction (eq 2). From these results, one may infer that vinyl ketones **V** are much more reactive toward a hydrofurylation than vinyl ketones **III**.

Two general mechanisms are well established in the literature to account for the gold-catalyzed hydroarylation of unsaturated substrates: inner-sphere *syn*-addition and outer-sphere *anti*-addition (Friedel−Crafts-type mechanism).[1c] Based on this, Hashmi and co-workers proposed the two catalytic cycles shown in Scheme 1 for hydrofurylation of vinyl ketones.[1b,2] Although the feasibility of these two mechanisms has been already well-discussed in the literature,[1] we will show in this study that the corresponding furyl functionalization is best

Scheme 1

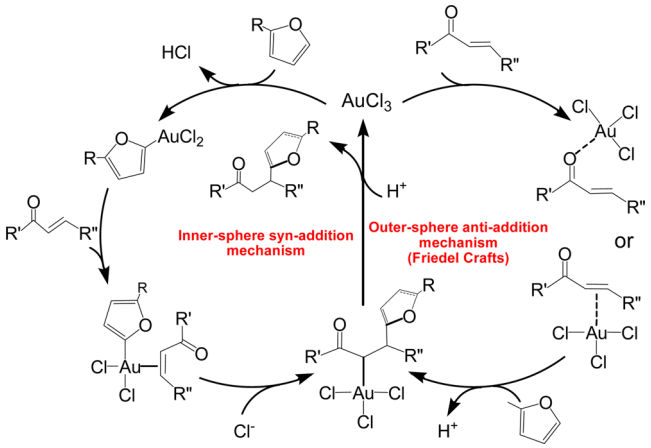

rationalized in terms of a novel third mechanism called "concerted electrophilic ipso-substitution" (CEIS) in which the gold-furyl σ-bond produced by furan auration acts as a nucleophile and attacks the protonated substrate via an outer-sphere mechanism (Scheme 2). In this study, we will show that the CEIS mechanism can be expanded to explain the $AuCl_3$-

Received: June 5, 2016
Published: October 17, 2016

ACS Publications © 2016 American Chemical Society

DOI: 10.1021/jacs.6b05742
J. Am. Chem. Soc. 2016, 138, 14599−14608

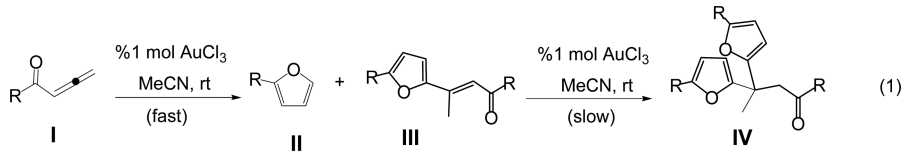

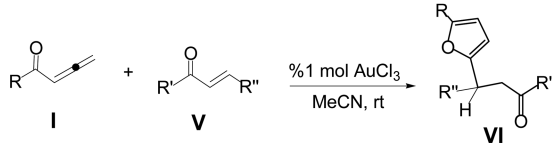

Scheme 2

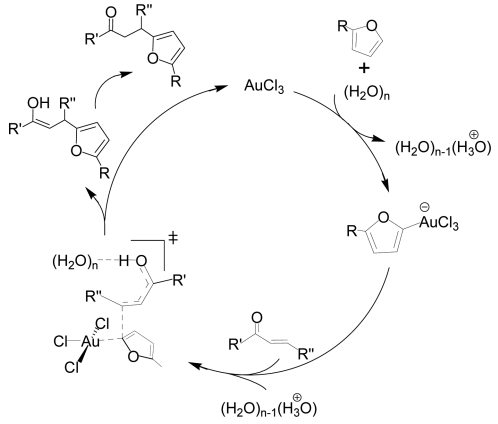

catalyzed reduction of ketones to alcohols and then to alkanes via a hydrofurylation process. The CEIS mechanism is expected to receive greater consideration as an important potential pathway for gold-catalyzed arene functionalization reactions in future studies.

RESULTS AND DISCUSSION

Hydroarylation of Allenyl Ketones. We began our investigation by addressing the question why the treatment of allenyl ketones with the $AuCl_3$ catalyst afforded a mixture of furan and furyl-substituted vinyl ketone in acetonitrile. In our computational modeling, penta-3,4-dien-2-one is used as the allene substrate. The calculations show that, consistent with the previous studies,[3d] the reaction starts with coordination of the terminal alkene of the allene substrate to the $AuCl_3$ followed by ring closure via transition structure $\mathbf{TS_{1-2}}$ to form cyclic intermediate **2** (Figure 1).

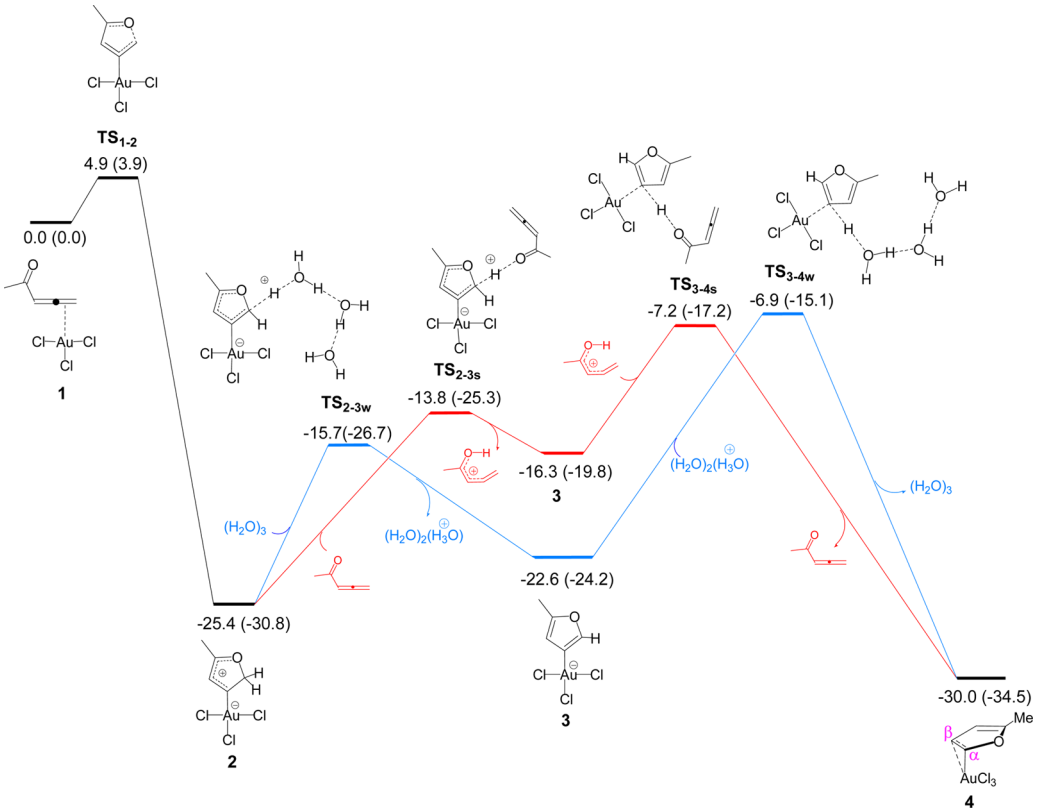

Figure 1. A calculated energy profile for $AuCl_3$-mediated ring closure of allenyl ketone followed by proton shift assisted by either water or an allenyl ketone substrate. The relative Gibbs and potential energies (in parentheses) obtained from the M06/BS2//B3LYP/BS1 calculations in acetonitrile are given in kcal/mol.

DOI: 10.1021/jacs.6b05742
J. Am. Chem. Soc. 2016, 138, 14599−14608

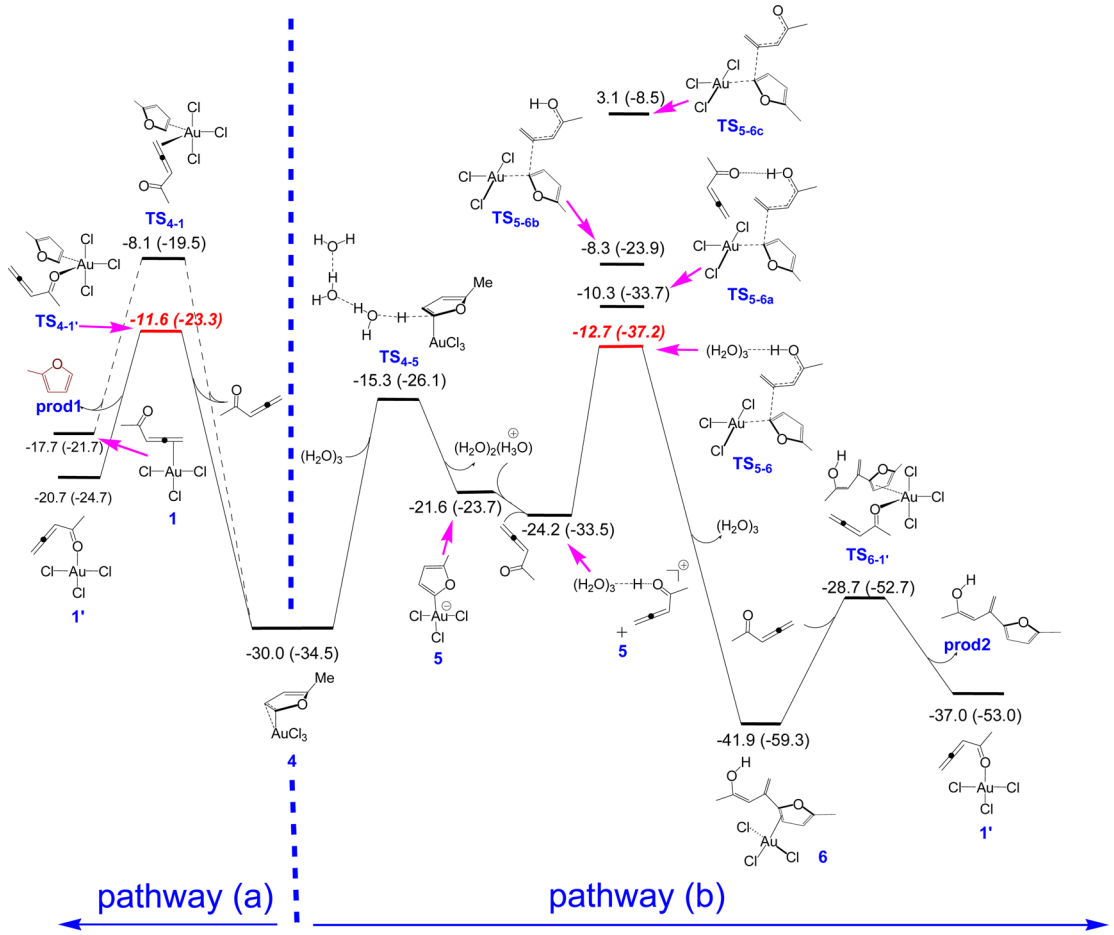

Figure 2. A calculated energy profile comparing the energetics of exchange of the ligated furan in **4** with the allenyl ketone substrate [pathway (a)] versus hydrofurylation of allenyl ketone **sub1** via the novel CEIS mechanism [pathway (b)]. The relative Gibbs and potential energies (in parentheses) obtained from the M06/BS2//B3LYP/BS1 calculations in acetonitrile are given in kcal/mol.

In the literature it is well-documented that H^+-migration processes in transition-metal-catalyzed reactions can be assisted by water molecules, bases, and anions.[3] The energy profile outlined in blue in Figure 1 shows the water-assisted 1,2-H shift process that occurs via a stepwise mechanism (deprotonation/protodeauration) with a free energy barrier of 18.5 kcal/mol.[4] Interestingly, we found that the allene substrate itself can also act as a proton transferring agent and facilitates the 1,2-H shift via a similar stepwise mechanism with an activation energy comparable to the water-assisted process ($\Delta G^{\ddagger}$ = 18.2 kcal/mol). However, the lower basicity of the allene substrate as compared to the water cluster renders the transition structure $\mathbf{TS}_{2-3s}$ higher in energy than transition structure $\mathbf{TS}_{2-3w}$ and transition structure $\mathbf{TS}_{3-4s}$ slightly lower in energy than transition structure $\mathbf{TS}_{3-4w}$. These findings imply a clear possibility of the protonated substrate being formed during the course of the catalytic reaction.[5]

The furan strongly coordinates to $AuCl_3$ in **4** with a binding energy of −42.9 kcal/mol. The high electrophilicity of $AuCl_3$ and the more nucleophilic character of the furan's α-carbon (C^{α}) result in an η^1 coordination mode for the gold−furan interaction; the Au−C^{α} distance (2.221 Å) is calculated to be 0.601 Å longer than the Au−C^{β} distance (2.822 Å). The NBO charge analysis indicates that the charge on the furan in **4** is +0.451, implying that this complex has some zwitterionic character.

Once **4** is formed, there are two pathways that compete with each other (Figure 2) to account for simultaneous formation of the furan and the dimer product as outlined in eq 1. In pathway (a), the furan group in **4** is exchanged with a substrate via an associative mechanism to afford an allene complex from which the ring-closure process repeats. In pathway (b), the furan complex can act as an active species for the hydroarylation reaction to give a furyl-substituted vinyl ketone as the initial dimer product.

For the exchange reaction, two trigonal-bipyramidal transition structures ($\mathbf{TS}_{4-1'}$ and $\mathbf{TS}_{4-1}$) are identified (Figure 2). In $\mathbf{TS}_{4-1'}$, the allene binds to the gold metal center via its carbonyl oxygen atom, while in $\mathbf{TS}_{4-1}$, the allene binds via its C═C π bond. Due to the oxophilicity of the gold(III) center, $\mathbf{TS}_{4-1'}$ is calculated to be lower in energy than $\mathbf{TS}_{4-1}$. This transition structure ($\mathbf{TS}_{4-1'}$) leads to formation of the O-bound linkage isomer **1′** which is about 3.0 kcal/mol more stable than π-bound isomer **1**.[6] It follows that the release of furan should proceed preferentially via the transformation of **4** → $\mathbf{TS}_{4-1'}$ → **1′** rather than **4** → $\mathbf{TS}_{4-1}$ → **1**. The exchange reaction (formation of **1′**) is found to be endergonic by +9.3 kcal/mol, suggesting that the electron-donating ability of furan is more significant than that of the allene substrate which consequently results in the furan binding more strongly than the allene substrate.

Pathway (b) starts with deprotonation of **4** by a water cluster via transition structure $\mathbf{TS}_{4-5}$ with a Gibbs energy barrier of

DOI: 10.1021/jacs.6b05742
J. Am. Chem. Soc. 2016, 138, 14599−14608

14.7 kcal/mol to afford 2-furyl complex **5** (Figure 2). Intriguingly, an unprecedented mechanism from this intermediate was detected in the C−C bond coupling process. We found that a deauration reaction can occur via an outer-sphere nucleophilic attack of the Au−C σ-bond to the central carbon of the allene substrate. However, this process becomes even more feasible if the allene substrate is protonated first. Indeed, the protonation increases the electrophilicity of the central allene carbon and causes the transition structure of the deauration reaction to be stabilized considerably, as evident from a comparison of relative Gibbs energies of $\mathbf{TS}_{5-6b}$ (−8.3 kcal/mol) and $\mathbf{TS}_{5-6c}$ (3.1 kcal/mol) (Figure 2). Furthermore, an extra stability to this transition structure can be provided by the hydrogen-bonding interaction of the protonated allene substrate with either another allenyl ketone or water molecules (transition structures $\mathbf{TS}_{5-6a}$ and $\mathbf{TS}_{5-6}$ in Figure 2).[7−9]

The product of the deauration reaction is a dienol intermediate (**6**) which undergoes another exchange reaction to give **1′** and **prod2**. Finally, the tautomerization of the released dienol (**prod2**) to the vinyl ketone product (**prod3**) completes the C−C coupling process (eq 3). In contrast to

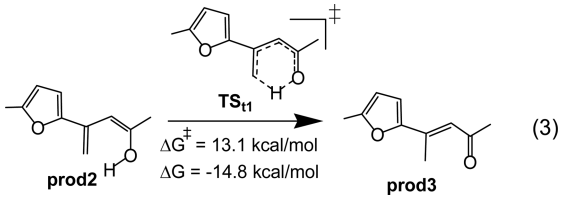

(3)

normal keto−enol tautomerization,[10] this process is found not to need any assistance from proton transferring agents (like water), and it directly takes place via the six-membered transition structure $\mathbf{TS}_{t1}$ with a Gibbs activation barrier of 13.1 kcal/mol (eq 3). The water-assisted proton transfer for this particular tautomerization is calculated to occur with higher activation energy (22.1 kcal/mol). It is worth noting that the favorability of the intramolecular proton transfer via $\mathbf{TS}_{t1}$ explains why only (*E*) isomers are formed as the initial products during the course of the hydroarylation process; however, the (*E*) isomers were also found to be thermodynamically more stable than the (*Z*) isomers (for instance, about 4.5 kcal/mol for organic product **prod3**).

The transition structures $\mathbf{TS}_{4-1'}$ and $\mathbf{TS}_{5-6}$ correspond to the highest energy points along pathways (a) and (b), respectively (Figure 2). The Gibbs energies of these two transition structures are fairly close, which might explain why allenyl ketones are catalyzed by $AuCl_3$ to produce a mixture of furan and a furyl-substituted vinyl ketone as the initial products.

Electronic Impact of the Aryl Ring. At this juncture, a question may arise as to why the 3-furyl complex **3**, which is formed during the ring-closure process (Figure 1), does not participate in the deauration reaction to form vinyl ketone **prod4** (Figure 3). Our calculations show that the transition structure for deauration of **3** ($\mathbf{TS}_3$) is 14.2 kcal/mol higher in energy than the analogous transition structure for deauration of **5** ($\mathbf{TS}_{5-6}$),[11] and starting from **3**, this process needs an activation energy as high as 24.1 kcal/mol (Figure 3). This result suggests that this type of deauration reaction is very sensitive to nucleophilicity of the aryl gold complex and is fast if the Au−C σ-bond is sufficiently nucleophilic. The lower nucleophilicity of **3** compared to **5** can be related to the generally accepted notion that the furan's β-carbon has a lower

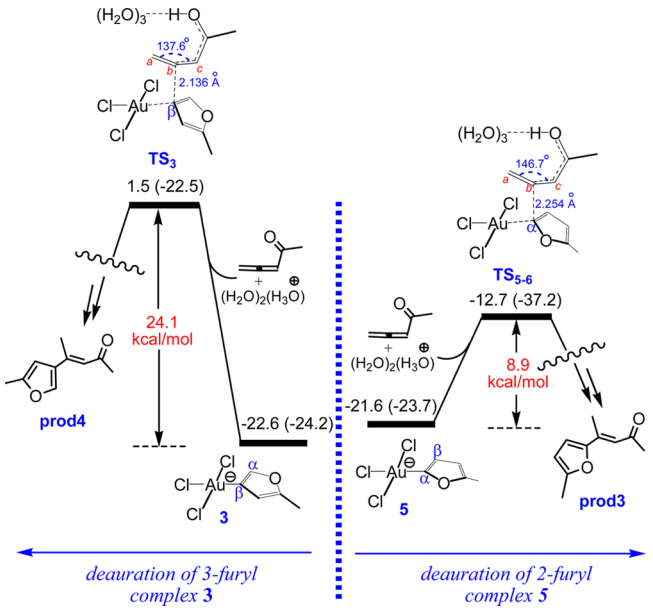

Figure 3. A calculated energy profile comparing the energetics of the CEIS mechanism starting from 3-furyl complex **3** and 2-furyl complex **5**. The relative Gibbs and potential energies (in parentheses) obtained from the M06/BS2//B3LYP/BS1 calculations in acetonitrile are given in kcal/mol.

nucleophilic character than the furan's α-carbon. The shorter C^b−C(furyl) distance in $\mathbf{TS}_3$ (2.136 Å) than in $\mathbf{TS}_{5-6}$ (2.254 Å) as well as the smaller C^a−C^b−C^c angle in $\mathbf{TS}_3$ (137.6°) than in $\mathbf{TS}_{5-6}$ (146.7°) (Figure 3) suggest a later transition structure for $\mathbf{TS}_3$, which further supports the lower nucleophilicity argument of **3**.

Alternative Mechanisms. As mentioned in the Introduction, gold-catalyzed hydroarylation of unsaturated compounds has been proposed to proceed through two potential mechanisms: (a) inner-sphere *syn*-addition and (b) outer-sphere antiaddition (Friedel−Crafts-type) (Scheme 1).[1g] Here, we compare the energetics of hydroarylation via these two mechanisms with the novel CEIS mechanism and show that these alternatives would not be involved in the C−C coupling process.

In order for the inner-sphere *syn*-addition pathway to start, one of the Cl^- ligands *cis* to the furyl ligand in **5** should be substituted by the allene substrate to form **7** (Figure 4). The released Cl^- can be further stabilized through hydrogen-bonding interaction with hydronium, as suggested by Boorman and Larrosa.[1h] After formation of **7**, the allene can easily insert into the Au−C(furyl) bond with a Gibbs activation barrier of 4.2 kcal/mol. Figure 4 shows that the hydronium-assisted substitution reaction is markedly endergonic (ΔG = +11.9 kcal/mol), resulting in all the stationary points on the inner-sphere *syn*-addition pathway to lie above the key transition structure of the CEIS mechanism ($\mathbf{TS}_{5-6}$), rendering the inner-sphere *syn*-addition pathway unfavorable.

It is proposed in the literature that the Friedel−Crafts-type (outer-sphere *anti*-addition) mechanism may start with the nucleophilic addition of furan to the oxygen-bound allene complex **1′** (Figure 5).[2] The transition structure for this process ($\mathbf{TS}_{1'-8}$) is calculated to be much higher in energy than the vital transition structures $\mathbf{TS}_{4-1'}$ and $\mathbf{TS}_{5-6}$, implying that the carbon−carbon coupling does not occur from this linkage isomer.

DOI: 10.1021/jacs.6b05742
J. Am. Chem. Soc. 2016, 138, 14599−14608

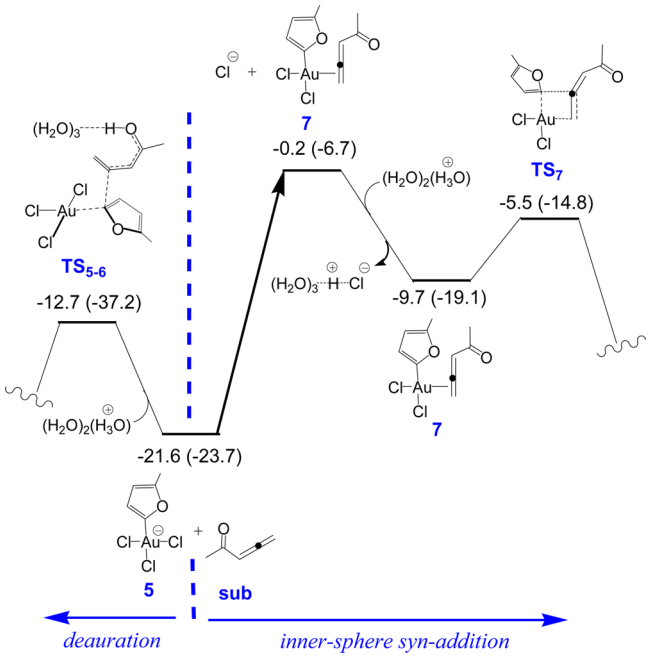

Figure 4. A calculated energy profile comparing the energetics of the CEIS mechanism versus the inner-addition *syn*-addition mechanism. The relative Gibbs and potential energies (in parentheses) obtained from the M06/BS2//B3LYP/BS1 calculations in acetonitrile are given in kcal/mol. The energy change of **7** on the energy profile is due to stabilization of the Cl^- anion by $(H_2O)_2(H_3O)^+$.

Another possibility for the Friedel–Crafts-type mechanism is that the furan nucleophilically attacks the π-complex **1** to afford **9**. The transition structure of this outer-sphere mechanism is about 2.1 kcal/mol above that of the ring-closure reaction via $\mathbf{TS_{1-2}}$. This result suggests that once **1** is formed, it is involved immediately in the ring closure and thus is less likely to undergo the Friedel–Crafts-type process.[12]

It follows from these results that although all the pathways may lead to a C–C coupling product, the reaction should preferentially proceed through the unprecedented CEIS mechanism in which the Au–C(furyl) σ-bond acts as a nucleophile and attacks the water-stabilized protonated allenyl ketone substrate (vide supra).

Hydroarylation of Vinyl Ketones. The next question is why allenyl ketones in the presence of vinyl ketones exhibit a different behavior and the hydroarylation reaction is catalyzed by $AuCl_3$ to give only ketones as the final product (eq 2). Intriguingly, the reason for this change can be rationalized based on the CEIS mechanism. The 2-furyl complex **5** is predicted to react more quickly with a vinyl ketone than an allenyl ketone. The overall activation barriers for the deauration of **5** by the vinyl ketones **sub2** and **sub3** via transition structures $\mathbf{TS_{5-10}}$ and $\mathbf{TS_{5-11}}$ are calculated to be 14.5 and 15.8 kcal/mol, respectively, which are lower in energy than that for the allenyl ketone **sub1** via $\mathbf{TS_{5-6}}$ (17.3 kcal/mol) (Figure 6). Also, the higher reactivity of vinyl ketones **sub2** and **sub3** does not allow the allenyl ketone to be involved in the exchange reaction with adduct **4** (Figure 2) to release the furan. Thus, as supported by the experiment, neither the furan nor the furyl-substituted vinyl ketone is predicted to be formed in the presence of the vinyl ketones. However, it should be noted that the reactivity of vinyl ketones is sensitive to the substituents at their β-position. For example, the vinyl ketone **prod3** in which its β positions are substituted by the methyl and furyl groups increases the activation barrier of the deauration process to 23.4

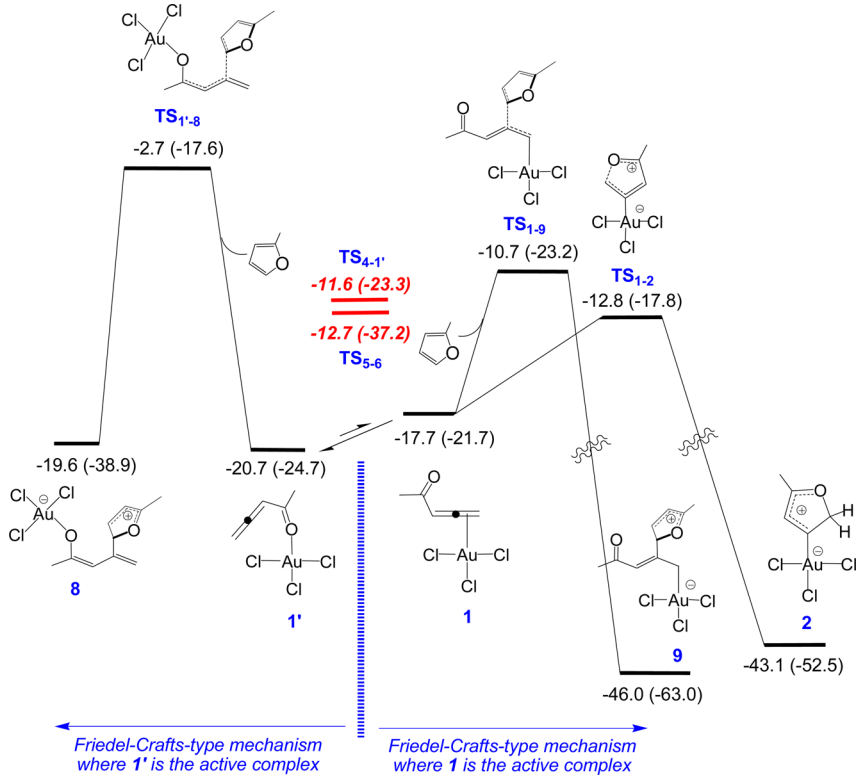

Figure 5. A calculated energy profile comparing the energetics of the CEIS mechanism versus Friedel–Crafts-type mechanism. The relative Gibbs and potential energies (in parentheses) obtained from the M06/BS2//B3LYP/BS1 calculations in acetonitrile are given in kcal/mol.

DOI: 10.1021/jacs.6b05742
J. Am. Chem. Soc. 2016, 138, 14599–14608

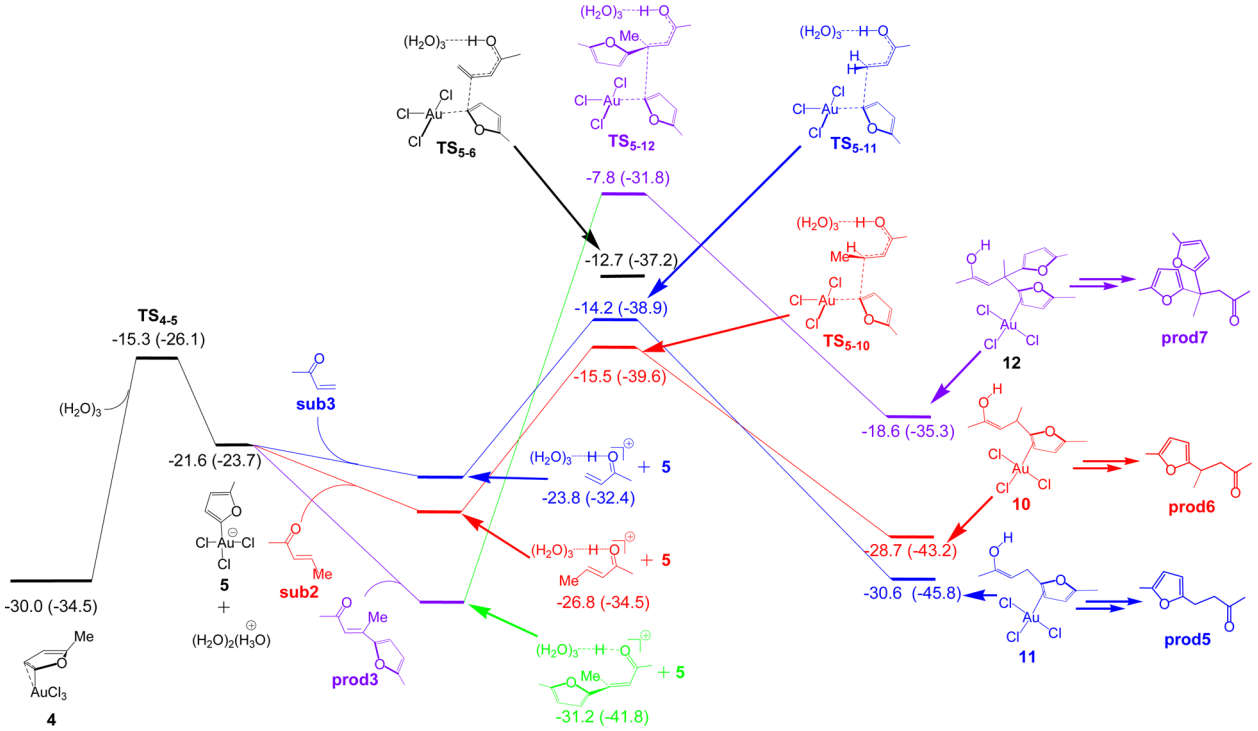

Figure 6. Energy profile of deauration step for allenyl ketone **sub1** and vinyl ketones **sub2**, **sub3**, and **prod3**. The relative Gibbs and potential energies (in parentheses) obtained from the M06/BS2//B3LYP/BS1 calculations in acetonitrile are given in kcal/mol.

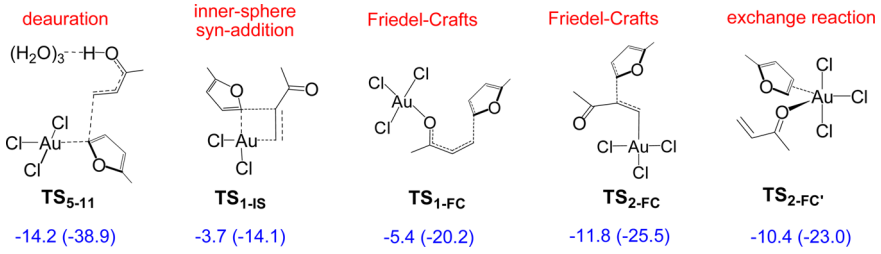

Figure 7. Relative energies of vital transition structures for hydrofurylation of vinyl ketone **sub3** catalyzed by $AuCl_3$. The relative Gibbs and potential energies (in parentheses) obtained from the M06/BS2//B3LYP/BS1 calculations in acetonitrile are given in kcal/mol.

kcal/mol and causes the transition structure $\mathbf{TS_{5-12}}$ to be 4.9 kcal/mol higher in energy than $\mathbf{TS_{5-6}}$. This result explains why when **prod3** is produced as the initial product, it slowly reacts with the furan to give the final product **prod7**. A plausible rationalization that may account for the lower reactivity of **prod3** is the steric effect of the β-substituents which does not allow the 2-furyl complex **5** to easily interact with the vinyl ketone in the transition structure.

An enol tautomer is the initial product of the deauration of the vinyl ketones. The enol form should undergo a tautomerization to afford a more stable keto form. This process which can be catalyzed by water molecules has been discussed previously in the literature and thus needs no further investigation in this study.[13]

To establish the favorability of the CEIS mechanism, the other mechanisms were also assessed for comparison. For example, our calculations for vinyl ketone **sub3** show that the vital transition structures of the inner-sphere *syn*-addition, the Friedel–Crafts-type, and the exchange reaction are all higher in energy than $\mathbf{TS_{5-11}}$, suggesting that the CEIS mechanism is favored over the others (Figure 7).

Catalytic Cycles for Cycloisomerization and Hydrofurylation of Allenyl and Vinyl Ketones. The catalytic cycles illustrated in Scheme 3 summarize the results of our investigations. Three catalytic processes are competing with each other to give either a furan (**prod1** in cycle 1), or a vinyl ketone (**prod3** in cycle 2), or a ketone (**prodn** in cycle 3). The stability of transition structures $\mathbf{TS_{4-1'}}$, $\mathbf{TS_{5-6}}$, and $\mathbf{TS_n}$ determines which catalytic cycle is preferred over the others. Since the energies of $\mathbf{TS_{4-1'}}$ and $\mathbf{TS_{5-6}}$ are quite similar, the catalytic cycles 1 and 2 are expected to be in operation with rate constants comparable to each other. Therefore, consistent with the experimental findings, in the absence of vinyl ketones, both products **prod1** and **prod3** should be formed simultaneously. The comparability of the $\mathbf{TS_{4-1'}}$ and $\mathbf{TS_{5-6}}$ energies is further corroborated by additional single-point calculations at the M06/BS3 and M06-D3/BS3 levels, where BS3 utilizes def2-QZVP for all atoms along with the effective core potentials including scalar relativistic effects for Au. The relative Gibbs energies of $\mathbf{TS_{4-1'}}$ and $\mathbf{TS_{5-6}}$ using M06/BS3 are −10.4 and −8.9 kcal/mol, respectively, while using M06-D3/BS3, they are −12.1 and −13.1 kcal/mol, respectively.

The presence of the vinyl ketones with nonbulky R and R′ substituents alters the situation and causes cycle 3 to proceed faster than cycles 1 and 2. In this case, $\mathbf{TS_n}$ is lower in energy than $\mathbf{TS_{4-1'}}$ and $\mathbf{TS_{5-6}}$, and the catalytic reaction only gives

DOI: 10.1021/jacs.6b05742
J. Am. Chem. Soc. 2016, 138, 14599–14608

Scheme 3

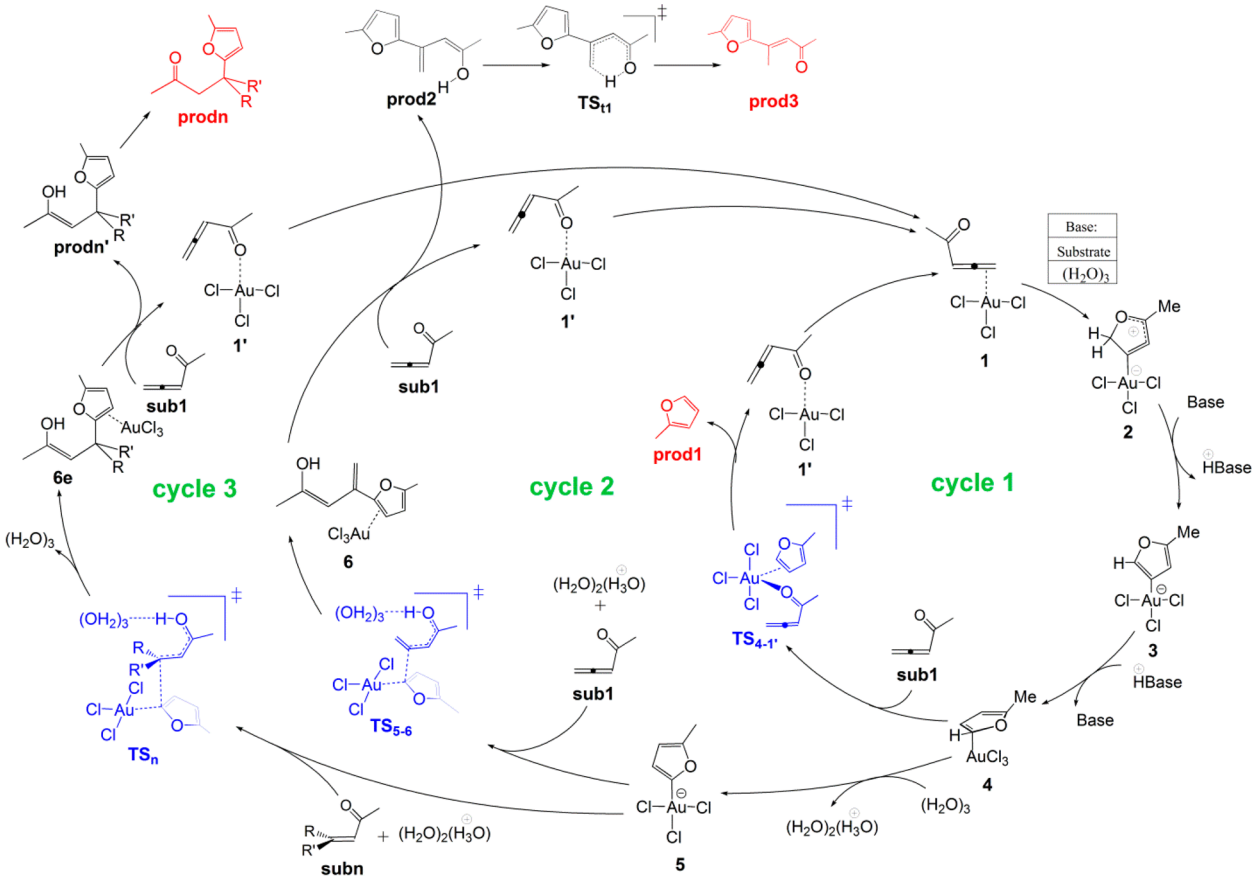

prod*n* as the final product. This argument is also supported by additional single-point calculations. For example, both M06/BS3 and M06-D3/BS3 levels for the vinyl ketone with R = Me and R′ = H predict that **TS$_n$** (**TS$_{5-10}$** in Figure 6) lies below **TS$_{4-1'}$** and **TS$_{5-6}$**; the relative Gibbs energies of **TS$_{5-10}$**, **TS$_{4-1'}$** and **TS$_{5-6}$** using M06/BS3 are −12.0, −10.4, and −8.9 kcal/mol, respectively, and using M06-D3/BS3 are −16.5, −12.1, and −13.1 kcal/mol, respectively.

However, it is worth noting that the bulkier R and R′ substituents such as R = Me and R′ = furyl render **TS$_n$** (**TS$_{5-12}$** in Figure 6) less stable than **TS$_{4-1'}$** and **TS$_{5-6}$**, and as such, cycles 1 and 2 are repeated much faster than cycle 3. In these circumstances, the initial products are **prod1** and **prod3**, and **prod*n*** is formed when the catalytic cycles 1 and 2 are fully completed.

Application of the CEIS Mechanism for Reduction of Ketones to Alkanes. Hashmi and co-workers also reported that aldehydes and ketones can react with 2 equiv of furans to give alkanes as the final products.[14] For example, they observed the production of **prod9** when the aldehyde substrate **sub4** is treated with furans in MeCN (eq 4). It is shown in the

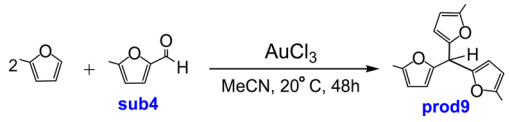

(4)

following that a similar CEIS mechanism can also operate appropriately to account for the AuCl$_3$-catalyzed condensation of two furans with an aldehyde. The reaction mechanism is illustrated based on the two sequential catalytic cycles given in Scheme 4. Figure 8 shows the calculated energy profile relating to these catalytic cycles. In both the catalytic cycles, adduct **4** serves as an active catalyst, and its deprotonation by a water cluster leads to formation of 2-furyl complex **5**. In cycle 4, the alcohol is produced through interaction of the Au−C σ-orbital of **5** with the C=O π^* orbital of the water-stabilized protonated ketone **sub4**. The reaction, which leads to formation of **prod8**, is endergonic by 3.0 kcal/mol (Figure 8). This result may explain why the alcohol product is not experimentally detectable. The hydroarylation reaction in cycle 4 proceeds with a calculated Gibbs energy barrier of 20.1 kcal/mol (Figure 8). The resultant alcohol subsequently gains a proton and produces the carbocation **15**. Due to the presence of the aryl rings, the benzylic carbocation **15** is found to be much more stable than the alcohol **prod8**. In cycle 5, intermediate **5** nucleophilically attacks the carbocation **15** via transition structure **TS$_{5-16}$**, affording the alkane product. Our calculations indicate that the deauration of **5** by carbocation **15** with a Gibbs activation barrier of 25.5 kcal/mol corresponds to the rate-limiting step for this 2-fold reaction.

It follows that the CEIS mechanism not only is capable of rationalizing hydroarylation of allenyl and vinyl ketones but also provides a consistent explanation for reduction of ketones to alkanes. This novel mechanism may have a wider application to hydroarylation of other substrates such as benzylic-propargylic alcohols, benzylic acetates, or vinyl aldehydes, a comprehensive investigation of which is the objective of ongoing theoretical projects in our group.[15]

DOI: 10.1021/jacs.6b05742
J. Am. Chem. Soc. 2016, 138, 14599−14608

Scheme 4

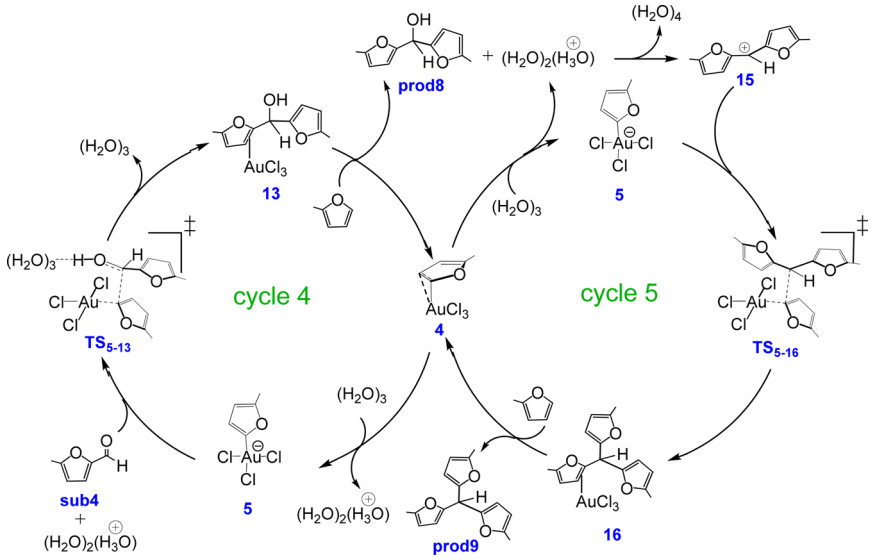

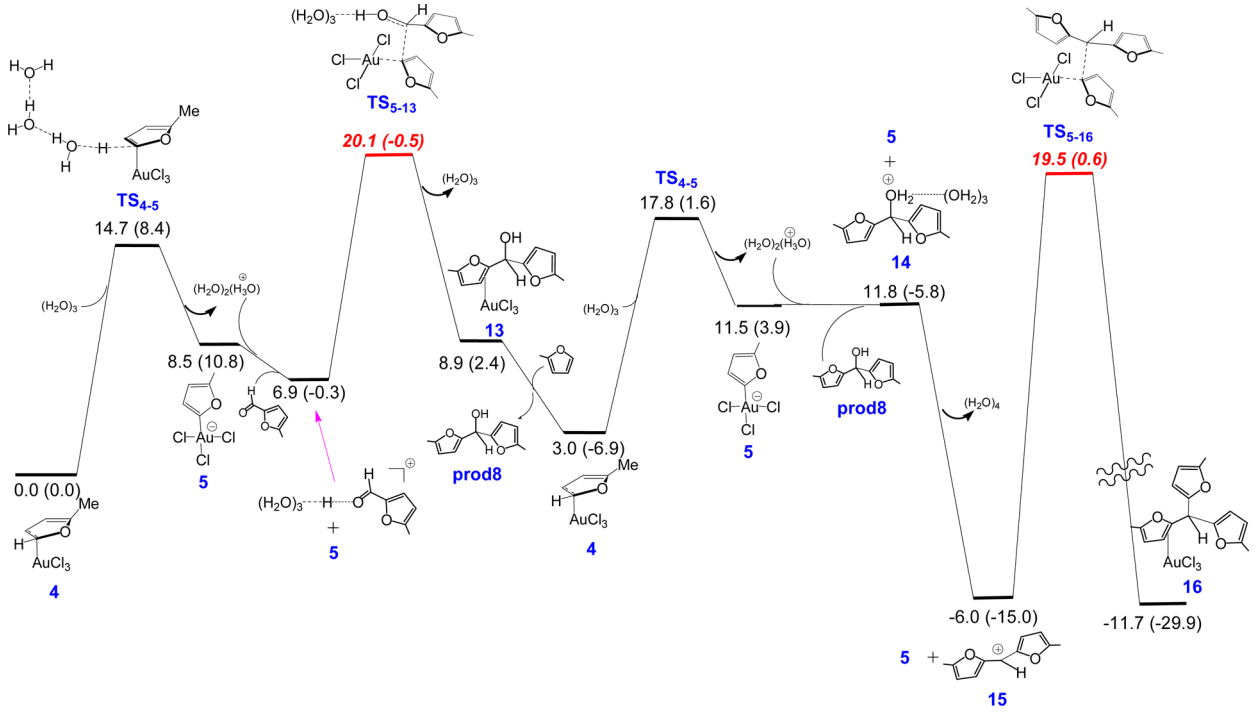

Figure 8. Energy profiles calculated for $AuCl_3$-catalyzed condensation of two furans with an aldehyde. The relative Gibbs and potential energies (in parentheses) obtained from the M06/BS2//B3LYP/BS1 calculations in acetonitrile are given in kcal/mol.

COMPUTATIONAL DETAIL

Gaussian 09[16] was used to fully optimize all the structures reported in this paper at the B3LYP level of density functional theory (DFT).[17] The effective-core potential of Hay and Wadt with a double-ξ valence basis set (LANL2DZ)[18] was chosen to describe Au. The 6-31G(d) basis set was used for other atoms.[19] A polarization function of ξ_f = 1.050 was also added for Au.[20] This basis set combination will be referred to as BS1. Frequency calculations were carried out at the same level of theory as those for the structural optimization. Transition structures were located using the Berny algorithm. Intrinsic reaction coordinate[21] calculations were used to confirm the connectivity between transition structures and minima. To further refine the energies obtained from the B3LYP/BS1 calculations, we carried out single-point energy calculations for all of the structures with a larger basis set (BS2) in acetonitrile using the CPCM[22] solvation model with the M06 DFT method. BS2 utilizes def2-QZVP along with the effective core potential including scalar relativistic effects[23] for Au and 6-311+G(2d,p) for other atoms. The potential and Gibbs free energies obtained from the M06/BS2//B3LYP/BS1 calculations in acetonitrile are used for interpreting the obtained results.

In calculations, the translational contribution to the entropy is evaluated based on the Thacker–Tetrode equation.[24] However, this contribution is suppressed upon going from the gas phase to a solvent, leading to an inadequate estimation of the Gibbs free energy changes, especially where the number of reactants is different from that of products. Recent theoretical studies[25] have used the formulation developed by Whitesides and co-workers[26] for obtaining more accurate values of the Gibbs free energy changes. The same formulation was used in this study to correct the entropic contributions. This formulation has been designed based on the fact

DOI: 10.1021/jacs.6b05742
J. Am. Chem. Soc. 2016, 138, 14599–14608

that the free space available for molecule movement is much smaller in solution than in the gas phase.

To assess how sensitive our results are to the dispersive effects for geometry optimizations and single-point energies, the structures of some selective transition states were reoptimized at the B3LYP-D3/BS1 level, and then their relative energies were re-evaluated with single-point calculations using the M06-D3/BS2 level of theory. The results show that there is a small dependence of the relative Gibbs energies on the dispersion. Using the M06/BS3//B3LYP/BS1 calculations, the relative energies of $\mathbf{TS}_{5-6}$, $\mathbf{TS}_{4-1'}$, $\mathbf{TS}_{1-9}$, $\mathbf{TS}_{1-2}$, $\mathbf{TS}_{1'-8}$, and $\mathbf{TS}_{7}$ are −12.7, −11.6, −10.7, −12.8, −2.7, and −5.5 kcal/mol, respectively. Using the M06-D3/BS2//B3LYP-D3/BS1 calculations, the relative Gibbs energies corrected are −13.1, −12.8, −11.8, −13.0, −3.8, and −6.7 kcal/mol, respectively. All the relative Gibbs free energies reported here have been corrected by the Whitesides approach.

CONCLUDING REMARKS

The significant insight that we have provided in this work is that Au−C(furyl) σ bonds serve as a nucleophile and attack easily the protonated unsaturated substrates such as allenyl ketones, vinyl ketones, ketones, and alcohols to form new C−C bonds. However, the nucleophilicity relies on the nature of the Au^{III}−C(furyl) σ bond; the binding of furan's α-carbon to gold makes the σ bond a strong nucleophile, while this is not the case for the binding of furan's β-carbon. We also found that the formation of the Au^{III}−C(furyl) σ bond is readily promoted by deprotonation of the Au^{III}−furan adduct by water or a substrate such as allenyl ketone. This new mechanism for carbon−carbon coupling might be applicable to many different substrates, and it has the potential to rationalize the reduction of many different species. It is quite significant that this is the first new mechanism proposed to explain gold-catalyzed nucleophilic addition reactions for some years, and it will be a useful partner to the two traditional mechanisms discussed in Scheme 2. This new mechanism that we have identified has the potential to provide a better understanding of other important examples in the literature and to rationalize different product formation.

ASSOCIATED CONTENT

Supporting Information

The Supporting Information is available free of charge on the ACS Publications website at DOI: 10.1021/jacs.6b05742.

A table giving Cartesian coordinates of all optimized structures along with energies (Table S1), an energy profile for hydroarylation catalyzed by $AuCl_3$, where allenyl ketone is activated by a second $AuCl_3$ (Figure S1), an energy profile comparing reactivity of furyl complexes **3** and **5** (Figure S2), an energy profile comparing the energetics of the ring-closure process and the nucleophilic attack of the 2-furyl complex **5** on the π-complex **1** (Figure S3), an energy profile comparing the energetics of the direct substitution reaction and the solvent-assisted substitution reaction (Figure S4), and an energy profile comparing the energetics of the nucleophilic attack on the central and terminal carbons of the allenyl ketone with the ring-closure process (PDF)

AUTHOR INFORMATION

Corresponding Authors

*hashmi@hashmi.de
*brian.yates@utas.edu.au
*alirezaa@utas.edu.au

Notes

The authors declare no competing financial interest.

ACKNOWLEDGMENTS

The authors gratefully acknowledge the generous allocation of computing time from the Australian National Computational Infrastructure and the University of Tasmania. A.H.B., Y.K., H.G., and A.A. appreciate financial support from the Iran Science Elites Federation.

REFERENCES

(1) (a) Hashmi, A. S. K.; Hutchings, G. J. *Angew. Chem., Int. Ed.* **2006**, *45*, 7896−7936. (b) Hashmi, A. S. K. *Chem. Rev.* **2007**, *107*, 3180−3211. (c) Gorin, D. J.; Toste, F. D. *Nature* **2007**, *446*, 395−403. (d) Patil, N. T.; Yamamoto, Y. *Chem. Rev.* **2008**, *108*, 3395−3442. (e) Gorin, D. J.; Sherry, B. D.; Toste, F. D. *Chem. Rev.* **2008**, *108*, 3351−3378. (f) Arcadi, A. *Chem. Rev.* **2008**, *108*, 3266−3325. (g) Bandini, M. *Chem. Soc. Rev.* **2011**, *40*, 1358−1367. (h) Boorman, T. C.; Larrosa, I. *Chem. Soc. Rev.* **2011**, *40*, 1910−1925. (i) Rudolph, M.; Hashmi, A. S. K. *Chem. Commun.* **2011**, *47*, 6536−6544. (j) Brand, J. P.; Li, Y.; Waser, J. *Isr. J. Chem.* **2013**, *53*, 901−910. (k) Gulevich, A. V.; Dudnik, A. S.; Chernyak, N.; Gevorgyan, V. *Chem. Rev.* **2013**, *113*, 3084−3213. (l) Yang, W.; Hashmi, A. S. K. *Chem. Soc. Rev.* **2014**, *43*, 2941−2955.

(2) Hashmi, A. S. K.; Schwarz, L.; Choi, J. H.; Frost, T. M. *Angew. Chem., Int. Ed.* **2000**, *39*, 2285−2288.

(3) For anion-, base-, and water-assisted proton transfer processes see: (a) Basallote, M. G.; Besora, M.; Durán, J.; Femández-Trujillo, M. J.; Lledós, A.; Máñez, M. A.; Maseras, F. *J. Am. Chem. Soc.* **2004**, *126*, 2320−2321. (b) Appelhans, L. N.; Zuccaccia, D.; Kovacevic, A.; Chianese, A. R.; Miecznikowski, J. R.; Macchioni, A.; Clot, E.; Eisenstein, O.; Crabtree, R. H. *J. Am. Chem. Soc.* **2005**, *127*, 16299−16311. (c) Davies, D. L.; Donald, S. M. A; Macgregor, S. A. *J. Am. Chem. Soc.* **2005**, *127*, 13754−13755. (d) Xia, Y.; Dudnik, A. S.; Gevorgyan, V.; Li, Y. *J. Am. Chem. Soc.* **2008**, *130*, 6940−6941. (e) Clot, E. *Eur. J. Inorg. Chem.* **2009**, *2009*, 2319−2328. (f) Kovács, G.; Lledós, A.; Ujaque, G. *Organometallics* **2010**, *29*, 3252−3260. (g) Kovács, G.; Lledós, A.; Ujaque, G. *Organometallics* **2010**, *29*, 5919−5926. (h) Krauter, C. M.; Hashmi, A. S. K.; Pernpointner, M. *ChemCatChem* **2010**, *2*, 1226−1230. (i) BabaAhmadi, R.; Ghanbari, P.; Rajabi, N. A.; Hashmi, A. S. K.; Yates, B. F.; Ariafard, A. *Organometallics* **2015**, *34*, 3186−3195.

(4) The concerted 1,2-H shift with an activation Gibbs energy of 24.2 kcal/mol is calculated to be less favorable than the water- or allenyl ketone-assisted process.

(5) The endergonicity calculated for the reaction $\mathbf{sub1}H^+$ + MeCN → **sub1** + $MeCNH^+$ (ΔG = 10.6 kcal/mol) suggests that protonation of the allenyl ketone in acetonitrile is feasible.

(6) An alternative mechanism for pathway (a) is that the furan in **4** is substituted by a MeCN (solvent) and subsequently the coordinated MeCN undergoes an exchange reaction with allenyl ketone to give **1′**. This variant was calculated to be slightly less favorable than the direct substitution reaction via $\mathbf{TS}_{4-1'}$ (for details see Figure S4).

(7) A mechanism in which allenyl ketone is activated by $AuCl_3$ was also investigated. This alternative pathway was found to be about 19.7 kcal/mol higher in energy than the one activated by the proton (for details see Figure S1).

(8) Although a complete proton transfer from $(H_2O)_2(H_3O)^+$ to allenyl ketone is endergonic by 6.3 kcal/mol, the hydrogen-bonding interaction between these two molecules is exergonic by −2.6 kcal/mol.

(9) Another variant of the carbon−carbon coupling is the nucleophilic attack of 2-furyl complex **5** on π-complex **1**. This alternative is unlikely to occur because it is about 10.3 kcal/mol less favorable than the ring-closure process (for details see Figure S3).

(10) (a) Yamabe, S.; Tsuchida, N. J. *J. Comput. Chem.* **2003**, *24*, 939−947. (b) Yamabe, S.; Tsuchida, N.; Miyajima, K. *J. Phys. Chem. A* **2004**, *108*, 2750−2757. (c) Cucinotta, C. S.; Ruini, A.; Catellani, A.; Stirling,

DOI: 10.1021/jacs.6b05742
J. Am. Chem. Soc. 2016, 138, 14599−14608

A. s. *J. Phys. Chem. A* **2006**, *110*, 14013−14017. (d) Cucinotta, C. S.; Ruini, A.; Catellani, A.; Stirling, A. *ChemPhysChem* **2006**, *7*, 1229−1234. (e) Freitag, M. A.; Pruden, T. L.; Moody, D. R.; Parker, J. T.; Fallet, M. *J. Phys. Chem. A* **2007**, *111*, 1659−1666. (f) D'Cunha, C.; Morozov, A. N.; Chatfield, D. C. *J. Phys. Chem. A* **2013**, *117*, 8437−8448.

(11) The experimentally observed product ratio in the dimerization reaction of allenyl ketone was reported to be 6000:1. This ratio corresponds to an energy difference of 5.1 kcal/mol for the energetic spans of the two free energy surfaces. However, the calculations predict an energy difference of 8.4 kcal/mol for these two pathways. This discrepancy might be partly attributed to nonprecise estimate of the entropy contribution which cannot be completely improved even when the Whitesides' formulation is employed. For details see the energy profile given in Figure S2.

(12) A strong evidence as to why the reaction is less likely to proceed via the Friedel−Crafts-type mechanism is that transition structure for the attack on the terminal carbon atom is about 0.7 kcal/mol lower in energy than that on the central carbon atom. The nucleophilic attack on the terminal carbon of allenyl ketone leads to a product that was not being detected experimentally (for details see Figure S5).

(13) (a) Yamabe, S.; Tsuchida, N.; Miyajima, K. *J. Phys. Chem. A* **2004**, *108*, 2750−2757. (b) Cucinotta, C. S.; Ruini, A.; Catellani, A.; Stirling, A. *ChemPhysChem* **2006**, *7*, 1229−1234. (c) Cucinotta, C. S.; Ruini, A.; Catellani, A.; Stirling, A. *J. Phys. Chem. A* **2006**, *110*, 14013−14017. (d) Freitag, M. A.; Pruden, T. L.; Moody, D. R.; Parker, J. T.; Fallet, M. *J. Phys. Chem. A* **2007**, *111*, 1659−1666. (e) D'Cunha, C.; Morozov, A. N.; Chatfield, D. C. *J. Phys. Chem. A* **2013**, *117*, 8437−8448.

(14) Hashmi, A. S. K.; Schwarz, L.; Rubenbauer, P.; Blanco, M. C. *Adv. Synth. Catal.* **2006**, *348*, 705−708.

(15) (a) Liu, J.; Muth, E.; Flörke, U.; Henkel, G.; Merz, K.; Sauvageau, J.; Schwake, E.; Dyker, G. *Adv. Synth. Catal.* **2006**, *348*, 456−462. (b) Mertins, K.; Iovel, I.; Kischel, J.; Zapf, A.; Beller, M. *Adv. Synth. Catal.* **2006**, *348*, 691−695. (c) Nair, V.; Abhilash, K. G.; Vidya, N. *Org. Lett.* **2005**, *7*, 5857−5859.

(16) Frisch, M. J.; Trucks, G. W.; Schlegel, H. B.; Scuseria, G. E.; Robb, M. A.; Cheeseman, J. R.; Scalmani, G.; Barone, V.; Mennucci, B.; Petersson, G. A.; Nakatsuji, H.; Caricato, M.; Li, X.; Hratchian, H. P.; Izmaylov, A. F.; Bloino, J.; Zheng, G.; Sonnenberg, J. L.; Hada, M.; Ehara, M.; Toyota, K.; Fukuda, R.; Hasegawa, J.; Ishida, M.; Nakajima, T.; Honda, Y.; Kitao, O.; Nakai, H.; Vreven, T.; Montgomery, J. A., Jr.; Peralta, J. E.; Ogliaro, F.; Bearpark, M.; Heyd, J. J.; Brothers, E.; Kudin, K. N.; Staroverov, V. N.; Kobayashi, R.; Normand, J.; Raghavachari, K.; Rendell, A.; Burant, J. C.; Iyengar, S. S.; Tomasi, J.; Cossi, M.; Rega, N.; Millam, J. M.; Klene, M.; Knox, J. E.; Cross, J. B.; Bakken, V.; Adamo, C.; Jaramillo, J.; Gomperts, R.; Stratmann, R. E.; Yazyev, O.; Austin, A. J.; Cammi, R.; Pomelli, C.; Ochterski, J. W.; Martin, R. L.; Morokuma, K.; Zakrzewski, V. G.; Voth, G. A.; Salvador, P.; Dannenberg, J. J.; Dapprich, S.; Daniels, A. D.; Farkas, O.; Foresman, J. B.; Ortiz, J. V.; Cioslowski, J.; Fox, D. J. *Gaussian 09*, Revision D.01; Gaussian, Inc.: Wallingford, CT, 2009.

(17) Zhao, Y.; Truhlar, D. G. *Acc. Chem. Res.* **2008**, *41*, 157−167.

(18) (a) Hay, P. J.; Wadt, W. R. *J. Chem. Phys.* **1985**, *82*, 270−283. (b) Wadt, W. R.; Hay, P. J. *J. Chem. Phys.* **1985**, *82*, 284−298.

(19) Hariharan, P. C.; Pople, J. A. *Theor. Chim. Acta* **1973**, *28*, 213−222.

(20) (a) Ehlers, A. W.; Böhme, M.; Dapprich, S.; Gobbi, A.; Höllwarth, A.; Jonas, V.; Köhler, K. F.; Stegmann, R.; Veldkamp, A.; Frenking, G. *Chem. Phys. Lett.* **1993**, *208*, 111−114. (b) Höllwarth, A.; Böhme, M.; Dapprich, S.; Ehlers, A. W.; Gobbi, A.; Jonas, V.; Köhler, K. F.; Stegmenn, R.; Veldkamp, A.; Frenking, G. *Chem. Phys. Lett.* **1993**, *208*, 237−240.

(21) (a) Fukui, K. *J. Phys. Chem.* **1970**, *74*, 4161−4163. (b) Fukui, K. *Acc. Chem. Res.* **1981**, *14*, 363−368.

(22) Barone, V.; Cossi, M. *J. Phys. Chem. A* **1998**, *102*, 1995−2001.

(23) Weigend, F.; Furche, F.; Ahlrichs, R. *J. Chem. Phys.* **2003**, *119*, 12753−12762.

(24) Gurney, R. W. *Introduction to Statistical Mechanics*, 1st ed.; McGraw-Hill Book Company: New York, 1949.

(25) (a) Ishikawa, A.; Nakao, Y.; Sato, H.; Sakaki, S. *Inorg. Chem.* **2009**, *48*, 8154−8163. (b) Zeng, G.; Sakaki, S. *Inorg. Chem.* **2011**, *50*, 5290−5297. (c) Zeng, G.; Li, S. *Inorg. Chem.* **2011**, *50*, 10572−10580. (d) Zeng, G.; Sakaki, S. *Inorg. Chem.* **2012**, *51*, 4597−4605. (e) Sakata, K.; Fujimoto, H. *J. Org. Chem.* **2013**, *78*, 12505−12512. (f) Ariafard, A. *Organometallics* **2014**, *33*, 7318−7324. (g) Guan, W.; Sakaki, S.; Kurahashi, T.; Matsubara, S. *ACS Catal.* **2015**, *5*, 1−10.

(26) Mammen, M.; Shakhnovich, E. I.; Deutch, J. M.; Whitesides, G. M. *J. Org. Chem.* **1998**, *63*, 3821−3830.

DOI: 10.1021/jacs.6b05742
J. Am. Chem. Soc. 2016, 138, 14599−14608